Psychoacoustic Characterization of Multirotor Drones in Realistic Flyover Maneuvers

Yupa Villanueva, R.M.; Merino Martinez, R.; Altena, A.; Snellen, M.

DOI
10.2514/6.2024-3015

Publication date
2024

Document Version
Final published version

Published in
30th AIAA/CEAS Aeroacoustics Conference (2024)

Aeroacoustics Conferences
June 4-7, 2024, Rome, Italy
30th AIAA/CEAS Aeroacoustics Conference (2024)

10.2514/6.2024-3015

Psychoacoustic characterization of multirotor drones in realistic flyover maneuvers

Renatto M. Yupa-Villanueva *, Roberto Merino-Martínez †, Anique Altena ‡, and Mirjam Snellen §
Delft University of Technology, Kluyverweg 1, 2629 HS Delft, the Netherlands

This study investigated the acoustic and psychoacoustic properties of five quadcopters drones during realistic flyover scenarios, utilizing a 64-microphone array for outdoor recordings. Acoustic analyses encompassed signal-to-noise ratio (SNR) values, time-frequency sound pressure levels, and noise spectra at overhead positions. An analysis based on A-weighted SNR revealed discernible drone noise despite background noise. Significant noise levels were observed up to 12 kHz. Harmonics of blade passage frequencies were evident, influencing noise spectra up to 1 kHz. Unlike traditional aircraft, drones' proximity to the ground limits the atmospheric absorption effects of high-frequency noise. A psychoacoustic analysis focused on sound quality metrics (SQMs) and annoyance assessment. SQMs exhibited consistent patterns across attributes, such as sharpness, tonality, roughness, and impulsiveness, with notable drone-specific perceptions. Different annoyance models indicated varying degrees of annoyance perception, with the Autel EVO II drone (lowest installation ratio, defined as the ratio between the drone diagonal size and the propeller diameter) perceived as the most annoying and the DJI Phantom 4 (heaviest) as the least one. Propeller positioning, represented by the parameter of installation ratio, correlated significantly with annoyance levels, suggesting an influence on both noise signature and psychoacoustic response. These findings highlight the importance of understanding the acoustic and psychoacoustic impact of drones, particularly in urban environments.

I. Introduction

Unmanned aerial vehicles (UAVs), commonly called 'drones', are currently of significant interest due to their extensive applications for sectors such as aerospace, logistics, transport, and environmental monitoring [1]. Nevertheless, despite all their benefits, it is widely accepted that their noise emissions constitute a prominent factor that could exert limitations to gain public acceptance and be commercially viable [2, 3]. For instance, according to Gwak *et al.* [4], small drones have been reported to be perceived as more annoying than road vehicles and conventional aircraft when exposed to the same sound pressure levels. This heightened annoyance can be attributed to several factors. Gwak *et al.* [4] related it to the occurrence of tones, and high-frequency content, Christian and Cabell [5] assign it to the "loitering" effect which appears when the drones fly in close proximity to the ground, and Zawodny *et al.* [6] stated that the increase in broadband noise levels, caused by drones operating within transitional Reynolds number regimes [7], dominates annoyance in the most perceptible frequency ranges for humans compared to tonal noise. Therefore, the study of drone noise has acquired significant attention since the public is concerned with the annoyance caused by drones in urban settings [8, 9]. Additionally, current regulation policies for drone noise certification are normally perceived as not reflecting the drone noise quality properly.

Current practices in the noise certification of aircraft rely on conventional metrics like equivalent sound pressure level ($L_{\mathrm{p,eq}}$), maximum A-weighted sound pressure level ($L_{\mathrm{p,A,max}}$), sound exposure level (L_{AE} or SEL), and effective perceived noise level (EPNL) [10]. However, these conventional metrics may not fully capture the acoustic aspects of unconventional aerial vehicles that contribute to human annoyance [11–14]. Studies have shown that EPNL and SEL inadequately address the perceptual effects of tonal components [11, 15]. Therefore, the use of psychoacoustic indicators, such as Sound Quality Metrics (SQMs) and Psychoacoustic Annoyance (PA) models, could assist in the design process of unconventional aerial vehicles for manufacturers. Similarly, these indicators could aid authorities in the certification process [12].

*PhD candidate, Aircraft Noise and Climate Effects, Faculty of Aerospace Engineering, R.M.YupaVillanueva@tudelft.nl
†Assistant professor, Aircraft Noise and Climate Effects, Faculty of Aerospace Engineering, R.MerinoMartinez@tudelft.nl
‡PhD candidate, Aircraft Noise and Climate Effects, Faculty of Aerospace Engineering, A.Altena@tudelft.nl
§Full professor, Aircraft Noise and Climate Effects, Faculty of Aerospace Engineering, M.Snellen@tudelft.nl

The acoustic and psychoacoustic characteristics of drones can be evaluated in controlled or non-controlled ambient conditions, such as anechoic chambers or outdoors, respectively. Likewise, different flight procedures can be assessed such as hovering, take-off, flyover, or landing. In controlled conditions and hovering flight procedures, Gwak *et al.* [4] investigated psychoacoustic aspects of multi-rotor UAV noise, identifying key factors influencing annoyance. Results showed that medium and large drones induced the highest annoyance, where sharpness played a crucial role in differentiating medium drones from civil aircraft, and that psychoacoustic indices alone could not explain the low annoyance of small drones. Alkmim *et al.* [16] proposed an experimental protocol for measuring the noise and directivity of a quadrotor drone in an anechoic chamber. They used a hemispherical microphone array setup to analyze directivity patterns, employing traditional sound metrics and SQMs, such as loudness, tonality, sharpness, roughness, and fluctuation strength (see section II.B). The authors compared psychoacoustic metrics at far-field positions using spherical acoustic holography and a head and torso simulator (HATS). Directivity patterns were fairly omnidirectional, with interference regions of low-noise emission, and estimated psychoacoustic metrics closely aligned with those computed using HATS measurements. Torija *et al.* [17] analyzed the impact of a hovering drone on urban soundscapes, finding that near busy roads, traffic noise masked the quadcopter's noise. In contrast, in quieter locations, perceived annoyance with drone noise surged up to 6.4 times higher than without drone noise.

Regarding different flight procedures, Ramos-Romero *et al.* [18] proposed a measurement and analysis framework for small UAV noise signatures during flyovers. Larger UAVs exhibited dominant broadband noise, while smaller ones displayed higher tonal noise contributions. The study identified the rear arc of polar directivity as the location of maximum noise radiation. Sound quality metrics, such as loudness, sharpness, fluctuation strength, and roughness offered insights into acoustic characteristics. Škultéty *et al.* [19] compared sound power levels of the quadcopters DJI Inspire 2 (3340 g - category C2) and Mavic 2 Pro (907 g - category C1) during flyovers, noting higher noise levels in the DJI Inspire in the 200 Hz to 20 kHz frequency range. A simulated UAV operation yielded A-weighted equivalent noise levels of 40 to 45 dBA. Ko *et al.* [20] focused on the impact of landing noise from UAV and urban air mobility (UAM) vehicles, emphasizing noise abatement through operational adjustments. Wake interaction effects significantly impacted the UAM vehicle's aerodynamic performance and noise characteristics. Additionally, a psychological noise impact analysis using SEL and Zwicker's PA metric [21] revealed the UAV's higher psychological impact despite lower physical noise. Ko *et al.* [22] presented a framework for auralizing multirotor noise during flyovers and takeoffs. Their study reported that modulation metrics, such as fluctuation strength and roughness, significantly impacted the predicted annoyance, with wind conditions and drone velocity also influencing psychoacoustic metrics. Moreover, Zwicker's PA metric [21] of the cross-type quadrotor was higher than that of the plus-type quadrotor. While previous research has offered valuable insights into the psychoacoustic impact of drones in real operational conditions, there remains a gap concerning the significance of impulsiveness under these circumstances. This metric has proven to be relevant in studies involving contra-rotating propeller configurations under controlled conditions, as demonstrated in research conducted in an anechoic chamber [23, 24]. In addition, most literature regarding drone noise measurements refers to stationary conditions typically performed in anechoic chambers, which are hardly representative of the actual operational conditions real drones would experience.

Therefore, the main goal of this manuscript is to investigate the noise emissions of drone flyovers in realistic maneuvers, as well as their psychoacoustic characteristics. Additionally, the recently-considered SQM impulsiveness [24, 25], is also computed and employed as input for annoyance calculation. In this way, an exploratory study considering five quadcopter drones in outdoor measurements under realistic operational conditions was conducted to evaluate the values of these indicators and establish meaningful connections between noise perception and the distinct characteristics of the drones. The influence of drone weight, volume, velocity, propeller diameter, and diagonal size between propellers are assessed.

II. Methodology

A. Experimental Setup

Acoustic data of five quadcopter drone flyovers were acquired during a measurement campaign at the Dutch military base of *Luitenant-generaal Bestkazerne* in October 2022 [26]. On this base, a large, open area with a grass surface was selected as the measurement location. This area was chosen as it was the optimal location to minimise the background noise from other activities on the base and to minimise reflections. An acoustic array of 64 microphones was employed for data acquisition. The microphones are arranged in an Underbrink spiral configuration [27] with a 4 m diameter. Acoustic foam and windshields cover the array and microphones to limit ground reflections and wind-induced noise. A picture of the array during the measurement campaign is shown in Figure 1. The data is collected using a sampling frequency of 50 kHz.

Fig. 1 Image of the microphone array during the measurement campaign

The five quadcopter drones used during the measurement campaign are depicted in Fig. 2. Relevant characteristics of these drones are depicted in Figure 3 and summarized in Table 1. The drones flew a straight line trajectory over the microphone array and during the flight both the altitude and flight velocity were kept as constant as possible. From each flyover, the GPS data of the drone was recorded. The relative distance from the drone to the array can, thus, be determined.

(a) DJI Mini 2. (b) DJI Mavic 3. (c) Autel EVO II. (d) DJI Phantom 3. (e) DJI Phantom 4.

Fig. 2 Drones used for the measurement campaign.

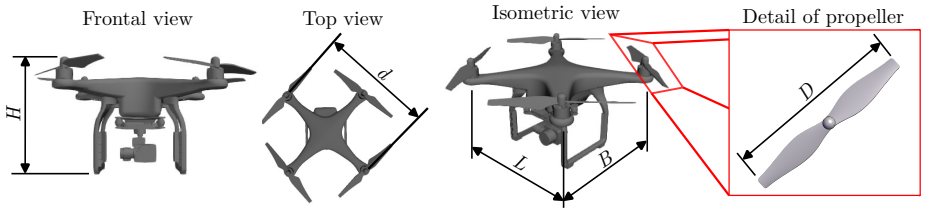

Fig. 3 Schematics depicting the main characteristic dimensions of both a drone and a propeller.

Table 1 Drone numbering and main characteristics.

Drone number	Drone model	Weight, W [g]	L x B x H [mm]	Propeller diameter, D [mm]	Diagonal size, d [mm]	Installation ratio, d/D [-]
1	DJI Mini 2	242	245 x 289 x 56	119	213	1.79
2	DJI Mavic 3	895	347.5 × 283 × 107.7	239	380	1.59
3	Autel EVO II	1191	424 x 354 x 110	230	397	0.56
4	DJI Phantom 3	1216	185 x 289 x 289.5	240	350	1.46
5	DJI Phantom 4	1380	289.5 x 289.5 x 196	240	350	1.46

B. Sound Quality Metrics and Psychoacoustic Annoyance Models

The Sound Quality Metrics (SQMs) describe the subjective perception of sound by human hearing, unlike the Sound Presure Level (L_p), which quantifies the purely physical magnitude of sound based on the acoustic pressure. Previous studies [28, 29] showed that these metrics better capture the auditory behavior of the human ear compared to conventional sound metrics typically employed in noise assessments. The five most commonly-used SQMs [30] are:

- Loudness (N): Subjective perception of sound magnitude corresponding to the overall sound intensity [31].
- Tonality (K): Measurement of the perceived strength of unmasked tonal energy within a complex sound [32].
- Sharpness (S): Representation of the high-frequency sound content [33].
- Roughness (R): Hearing sensation caused by sounds with modulation frequencies between 15 Hz and 300 Hz [34].
- Fluctuation strength (FS): Assessment of slow fluctuations in loudness with modulation frequencies up to 20 Hz, with maximum sensitivity for modulation frequencies around 4 Hz [35].

Additionally, a sound quality metric called impulsiveness (I) is also used in this work. This metric assesses the loudness N over time to quantify the degree of impulsive content within a sound, as specified by Willemsen and Rao [36]. It was included in the analysis due to its importance in propeller-driven aircraft, such as helicopters [37], and quadcopters [25]. The six sound quality metrics (SQMs) were computed over time. To evaluate the sound quality through single quantities, the 5th percentile values were considered. These values represent the level of each SQM exceeded during 5% of the total recording time (reported as subindex *5*). It is worth noting that the single value of impulsiveness represents the cumulative impulsive content, denoted as I_N.

The psychoacoustic annoyance (PA) models proposed by Zwicker and Fast [38], More [39], and Di *et al.* [40] used in this work combine the 5th percentile values of Sound Quality Metrics (SQMs) into a single global metric. The general expression for these PA models follows the Equation 1. The terms ω_S, ω_{FR} and ω_T are computed according to the Equations 2, 3 and 4, respectively. As can be noticed, these terms account for the effect of the SQMs through the 5th percentile values. Additionally, the coefficients C_0 to C_3 for each PA model are listed in Table 2 [29].

$$PA = N_5 \left(\sqrt{C_0 + C_1 \omega_S^2 + C_2 \omega_{FR}^2 + C_3 \omega_T^2} \right). \tag{1}$$

$$\omega_S = \begin{cases} 0.25(S_5 - 1.75)\log_{10}(N_5 + 10), & \text{for} \geq 1.75 \\ 0, & \text{for} < 1.75. \end{cases} \tag{2}$$

$$\omega_{FR} = \frac{2.18}{N_5^{0.4}}(0.4FS_5 + 0.6R_5). \tag{3}$$

$$\omega_T = \begin{cases} 0, & \text{for the model by Zwicker and Fastl [38]} \\ (1 - e^{-0.29N_5})(1 - e^{-5.49K_5}), & \text{for the model by More [39]} \\ \frac{6.41}{N_5^{0.52}} K_5, & \text{for the model by Di et al. [40].} \end{cases} \tag{4}$$

Table 2 Coefficients for the PA models based on 5th percentile values.

PA model	C_0	C_1	C_2	C_3
Zwicker and Fastl [38]	0	1	1	0
More [39]	-0.16	11.48	0.84	1.25
Di et al. [40]	0	1	1	1

Unlike the PA models based on 5th percentile values described above, Willemsen and Rao [36] developed a PA model combining not only the 5th-percentile values of loudness and roughness but also the median value of sharpness S_{50} and the cumulative impulsive content I_N, as shown in Equation 5. For this model, the term I_N is computed by Equation 6. N_i is the instantaneous loudness at data sample i of the loudness versus time signal. The term $N_{b,i}$ is the loudness of the non-impulsive components of the sound at data sample i. This non-impulsive, or baseline, loudness is calculated from the 95th percentile of the loudness over a moving 1-second block of time.

$$PA = 27.73 + 1.24I_N + 0.86N_5 \cdot S_{50} + 1.81R_5. \tag{5}$$

$$I_{\mathrm{N}} = \frac{1}{M}\sum_{i=1}^{M}[(N_i - N_b, i)] \tag{6}$$

All the SQMs (except for impulsiveness which was calculated with a code developed in-house) and the PA metrics were computed using the open-source MATLAB toolbox SQAT (Sound Quality Analysis Toolbox) v1.1 [41].

C. Drone Trajectories and Sound Level Correction

The original three-dimensional trajectory of each drone is depicted in Figure 4, where (x,y,z)=(0,0,0) corresponding to the microphone position. To ensure fair comparison of acoustic and psychoacoustic results, a trajectory-based correction for altitude differences (z-coordinate) is applied, as illustrated in Figure 5. This correction aligns all trajectories to a standardized altitude of 30.5 m, which corresponds to the mean altitude of the drones. Derived from the equation for sound propagation in a homogeneous atmosphere (Equation 7), it includes $L_{\mathrm{p,source}}\,(r,t)$ for noise source, $\sigma_{\nabla}\,(t)$ and σ_{α} for spherical spreading and atmospheric absorption losses, and σ_{ground} for ground reflection corrections. Since the microphones are at relatively low altitudes, only differences in spherical spreading losses are considered. Applying Equation 7 to both the original and corrected trajectories allows the derivation of Equation 8, which quantifies the sound level correction due to altitude differences. Here, z_{old} and z_{new} represent original and corrected altitudes, respectively, with ΔL_p being negative for $z_{\mathrm{old}} < z_{\mathrm{new}}$ and positive vice versa, thus partially accounting for differences in measuring distances. Table 3 presents the relatively small sound level corrections, with the maximum correction being -1.47 dB for the Autel Evo II drone.

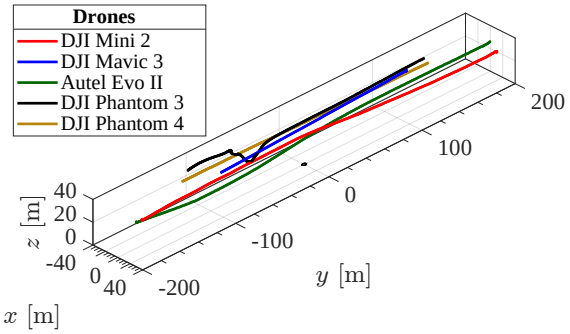

Fig. 4 Original three-dimensional trajectories.

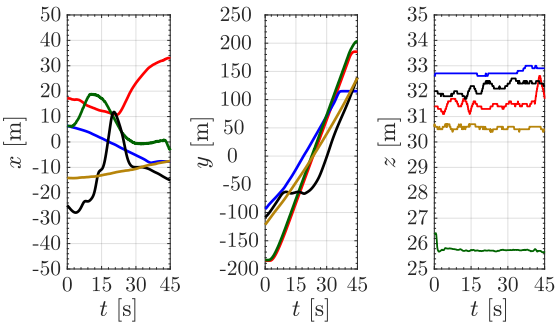

Fig. 5 Coordinates (x,y,z) along time for each drone flight path.

$$L_{\mathrm{p,mic}}(t) = L_{\mathrm{p,source}}(r,t) - \sigma_{\nabla}(t) - \sigma_{\alpha} - \sigma_{\mathrm{ground}}, \tag{7}$$

$$\Delta L_{\mathrm{p}} = 20\log_{10}\left(\frac{z_{\mathrm{old}}}{z_{\mathrm{new}}}\right) \tag{8}$$

Table 3 Sound level correction for each drone.

Drone number	Drone model	Sound level correction [dB]
1	DJI Mini 2	0.27
2	DJI Mavic 3	0.61
3	Autel EVO II	-1.47
4	DJI Phantom 3	0.44
5	DJI Phantom 4	0.01

III. Results and discussion

A. Acoustic Analysis

1. Signal-to-Noise-Ratio

The Signal-to-Noise Ratio (SNR), expressed as unweighted and A-weighted versions for each drone, is shown in Figure 6. This parameter is computed by subtracting the overall sound pressure level of background noise measurements from each drone's noise measurement. In the case of the A-weighted SNR, the same procedure is applied, but considering the A-weighted values for both the drone's noise measurement and the background noise instead. This allows for a quantitative verification of whether the sound produced by each drone, after applying the spreading sound-based correction, remains noticeable. Additionally, the maximum value of A-weighted SNR for each drone is used to determine when the drone is directly above the microphone (overhead position). The A-weighted version of the SNR is selected since it accurately represents the sensitivity of the human ear. Furthermore, it can be seen that the maximum value technically matches the time at which the overhead position occurs, with the exception of the drone 'DJI Phantom 4'. This finding can be understood as reasonable since the altitude of the drone is relatively low (30.5 m), resulting in approximately 0.09 seconds required for the sound wave to travel from the drone to the microphone, assuming a speed of sound of 343 m/s at 20°C. However, this behavior could vary depending on the position of the propeller in relation to the microphone, as drones possess polar and azimuthal noise directivity. Henceforth, for further analyses, 20 seconds of the entire measurement, comprising 10 seconds before and 10 seconds after the time of maximum A-weighted SNR for each drone, are considered. Henceforth, this time is denoted as t_{overhead}.

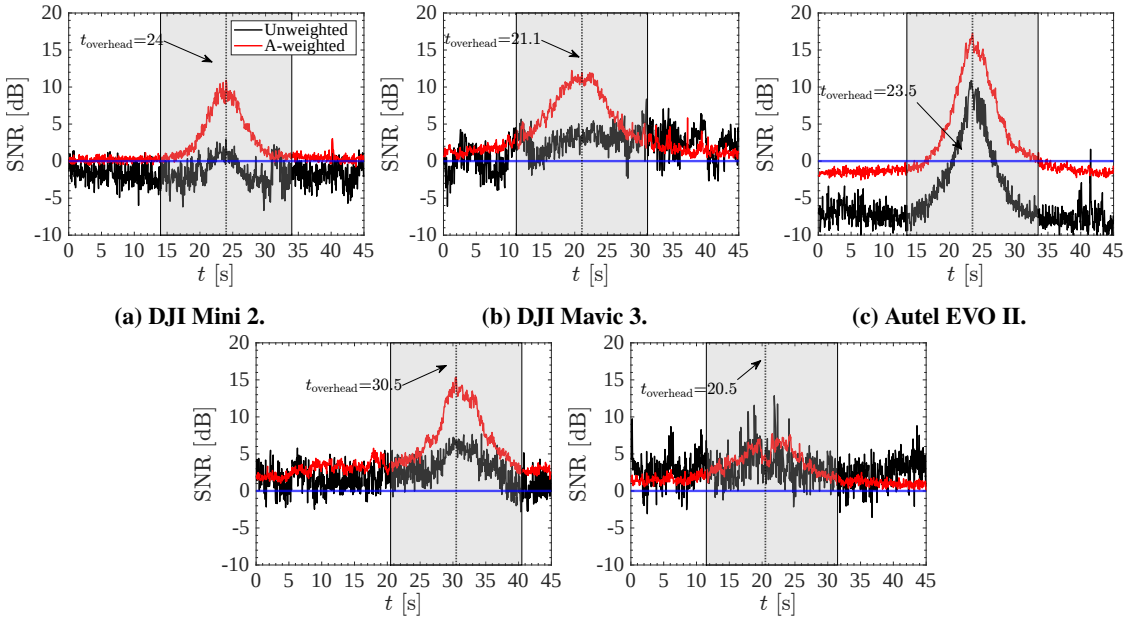

(a) DJI Mini 2. **(b) DJI Mavic 3.** **(c) Autel EVO II.**

(d) DJI Phantom 3. **(e) DJI Phantom 4.**

Fig. 6 Signal-to-noise ratio corresponding to each drone.

2. Sound Pressure Levels in Time-Frequency Domain

The time-frequency characteristics of each drone are analyzed through their respective spectrograms, as depicted in Figure 7. For each measurement, 20 s of recording time were used. The spectrograms are calculated using 5000 samples per time block with Hanning windowing and a 50% data overlap. With these parameters, the frequency resolution Δf is 10 Hz. The frequency range of interest for this research extends from 20 Hz to 20 kHz. The spectrograms are centered around the t_{overhead}. It can be noticed that similar patterns are observed between each drone not only corresponding to low-frequency noise but also in high-frequency noise up to 12 kHz, with the exception of the DJI Phantom 4 which presents higher noise levels up to 2.5 kHz. The high-frequency content could be explained by blade self-noise phenomena with turbulent boundary layer trailing edge noise [42], installation effects due to the interactions between adjacent rotors [43], and the electric motors due to force pulses as the magnets and armature interact [44].

The acoustic signature generated by drones is typically composed of multiple complex tones at the harmonics of the blade passage frequency (BPF) [4, 42–44]. This behaviour can be noted in Fig. 8, where the harmonics of the BPF are concentrated up to 1 kHz. Additionally, it is important to mention that ambient weather conditions influence the drone noise levels and the signatures in frequency and time domain [45]. For example, the presence of wind gusts in outdoor conditions makes the rotors of the drones vary their rotational speeds to maintain the vehicle in a stable attitude [42]. Due to these operational conditions, the amplitude of the tonal components decreases and the spectral content of the higher BPFs at higher frequencies suffers from dispersion [44].

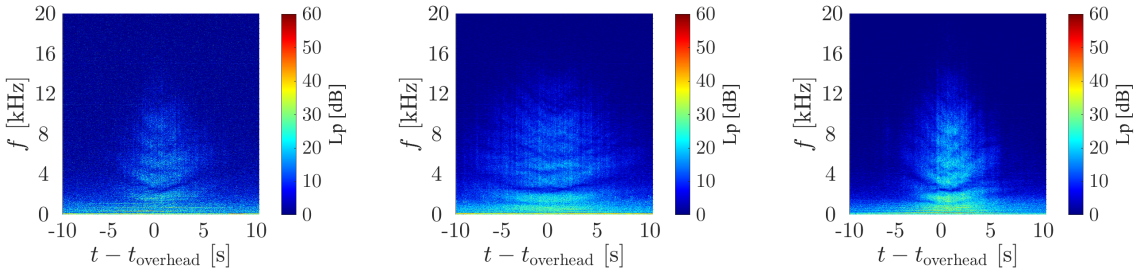

(a) DJI Mini 2. **(b) DJI Mavic 3.** **(c) Autel EVO II.**

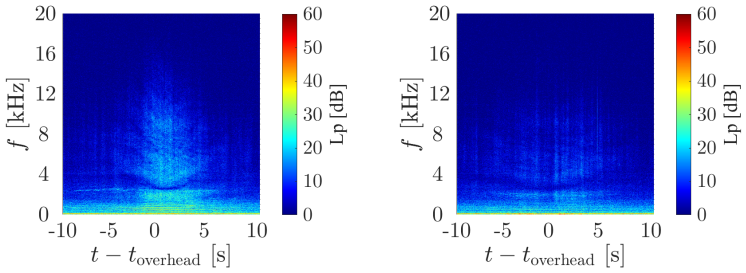

(d) DJI Phantom 3. **(e) DJI Phantom 4.**

Fig. 7 Spectrograms during the flight missions computed from 0 Hz to 20 kHz.

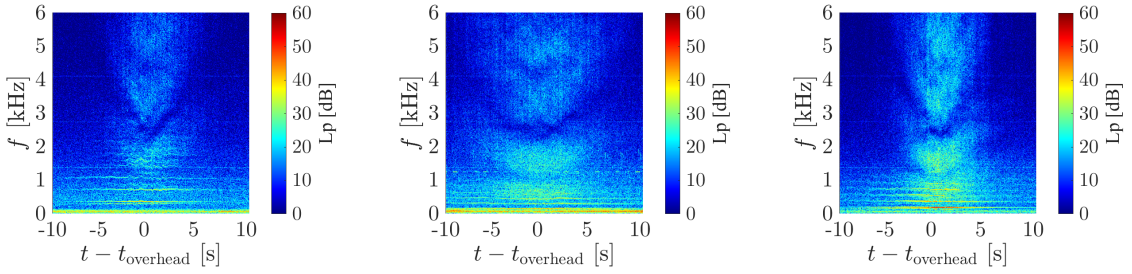

(a) DJI Mini 2. **(b) DJI Mavic 3.** **(c) Autel EVO II.**

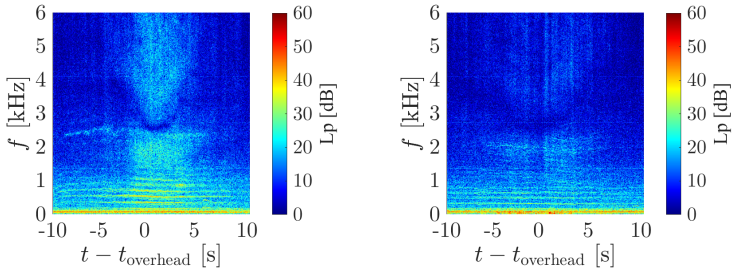

(d) DJI Phantom 3. **(e) DJI Phantom 4.**

Fig. 8 Spectrograms during the flight missions computed from 0 Hz to 6 kHz.

3. Noise Spectra at Overhead Position

The noise spectra computed at the overhead position for each drone are illustrated in Fig. 9, along with the background noise for comparison purposes. It can be identified that the background noise overshadows the noise produced by the drones by approximately up to 100 Hz. Additionally, it is evident that the harmonics of the Blade Passage Frequencies (BPFs) are predominantly noticeable up to 1 kHz. However, beyond 1 kHz, these harmonics become less discernible. Nevertheless, it is worth noting that the presence of high-frequency content has been identified as a significant contributor to noise annoyance [43]. In contrast to conventional fixed-wing aircraft, which typically operate around 400 m above the measurement point [15], drones operate at much lower altitudes, in this case, approximately 30.5 m over the microphone. Consequently, the atmospheric absorption, which usually mitigates high-frequency noise, is less effective for drones due to their proximity to the ground. Torija and Clark [23] compared the noise spectra between conventional aircraft and drones, emphasizing that drones exhibit higher levels of high-frequency content compared to conventional aircraft.

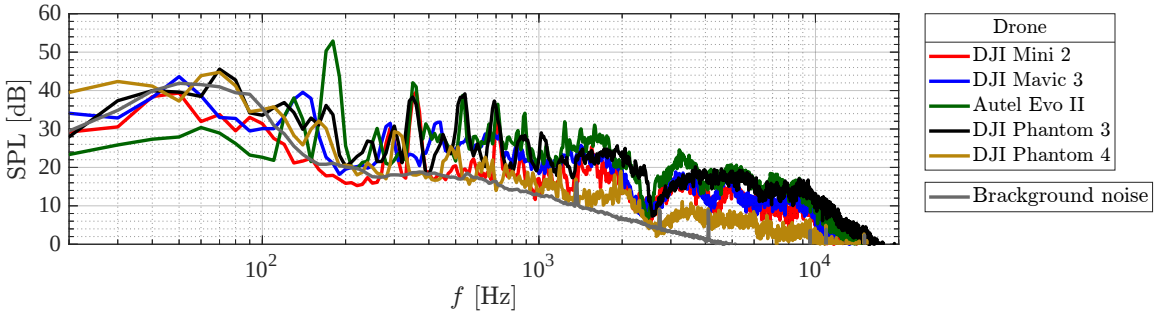

Fig. 9 Spectra computed for the overhead position for each drone. Background noise is also included for the sake of comparison.

B. Psychoacoustic Analysis

1. Sound Quality Metrics

The Sound Quality Metrics (SQMs) expressed as violin plots of each metric for each drone are presented in Figure 10. These plots show local density estimates corresponding to the transient values of each SQM, basic summary statistics inherent in box plots, as well as the 5th percentile values. The density trace is plotted symmetrically to the left and the right of the (vertical) box plot and it is computed following Equation 9. The term $d(x|h)$ represents the location density at a point x as the fraction of the data values per unit of measurement. The parameter n is the sample size, h is the interval width, and ith is one when the ith data value is in the interval $[x - h/2, x + h/2]$ and zero otherwise.

$$d(x|h) = \frac{\sum_{i=1}^{n} \delta_i}{nh} \tag{9}$$

Sound quality metrics such as sharpness, tonality, roughness, and impulsiveness exhibit similar transient density trace patterns, suggesting a consistent auditory signature across these attributes. However, the same coherence was not observed with loudness and fluctuation strength, as they fail to demonstrate comparable transient density trace patterns. Analyzing the 5th percentile values, the heaviest drone (DJI Phantom 4) is characterized as the 'harshest', 'least sharp', and 'quietest' achieving sound quality values of 0.012 vacil, 1.9 acum and 5.2 sone, respectively. Conversely, the lightest drone (DJI Mini 2) is perceived as the 'sharpest', 'least harsh', and 'least impulsive' with values of 2.1 acum, 0.006 vacil and 1.20 sone, respectively. On the other hand, the drone with the lowest installation ratio d/D (Autel Evo II) is found to be the 'loudest' (10 sone), 'most tonal' (0.142 t.u.), 'most beating' (0.234 asper), and 'most impulsive' (1.71 sone). Additionally, one of the drones with the largest propeller diameter (DJI Phantom 3) is perceived as the 'least tonal' (0.099 t.u.). To provide a comprehensive evaluation of the SQM in relation to each drone, Table 4 displays the 5th percentile values as well as the cumulative impulsive content I_N as a single indicator, as proposed by Willemsen and Rao [36].

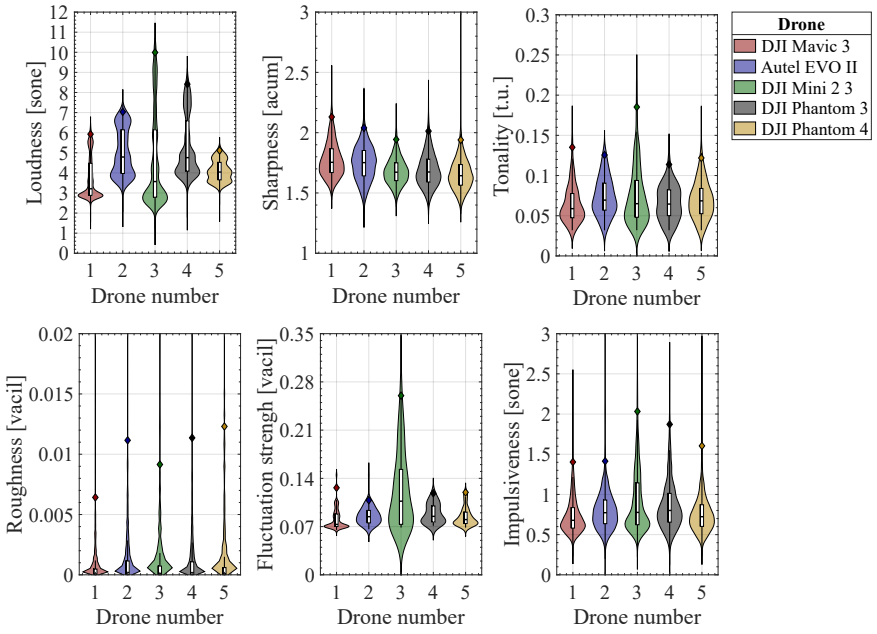

Fig. 10 Density traces of instantaneous values of sound quality metrics and their 5th percentile values.

Table 4 Summary of 5th percentile values of the six SQM for each drone, including I_N.

Drone number	Drone model	Sound quality metrics						
		L_5 [sone]	S_5 [acum]	K_5 [tu]	R_5 [vacil]	FS_5 [asper]	I_5 [sone]	I_N [sone]
1	DJI Mini 2	5.7	2.055	0.110	0.003	0.106	1.20	0.28
2	DJI Mavic 3	6.8	1.987	0.116	0.006	0.105	1.22	0.35
3	Autel EVO II	9.3	1.878	0.142	0.005	0.234	1.71	0.46
4	DJI Phantom 3	8.1	1.946	0.099	0.007	0.113	1.54	0.42
5	DJI Phantom 4	4.9	1.877	0.113	0.006	0.116	1.24	0.32

2. Psychoacoustic Annoyance

Figure 11 presents the instantaneous values of the normalized psychoacoustic annoyance computed by the PA models of Zwicker and Fast [38], More [39], and Di et al. [40]. The Willemsen and Rao [36] model was designed to compute a single value. Therefore, the annoyance from this model was not included in this figure. The normalization process involved dividing the instantaneous annoyance values by the maximum value for each PA model and for each drone. Additionally, the distance between the drone's flight path and the microphone is plotted, with its values corresponding to the right side axis of each figure. Alongside the distance curve, the transient velocity magnitude of each drone is shown, filled with a 'jet' color map. The velocity magnitude is calculated as the square root of the sum of the squares of the velocity components dx/dt, dy/dt, and dz/dt. It is clear that the distance decreases as the drones approach the microphone and increases as they move away. Additionally, it can be seen that the predicted psychoacoustic annoyance presents an opposite behavior, reaching maximum values when the drone is directly overhead, suggesting a strong dependence on distance. Moreover, the instantaneous annoyance values show similar trends for each PA model. However, some peak-type variations around the overhead position (minimum distance) can be noticed. For example, the annoyance peaks observed from the drones 'DJI Mavic 3' and 'Autel EVO II' after the overhead position seem to be related to a sudden increase in the drone velocity. However, the velocity of the drone 'DJI Mini 2' is technically constant, yet some variation in annoyance peaks can be noticed before and after the overhead position. Therefore, these peaks do not seem to be strictly related to drone velocity. Nevertheless, it is worth highlighting that using an Eulerian approach (fixed position receiver) as adopted in this investigation, the acoustic pressure used to compute the annoyance takes into account propagation effects. Consequently, a Lagrangian approach (receiver attached to the moving source) could help discern variations in annoyance values due to changes in drone velocity.

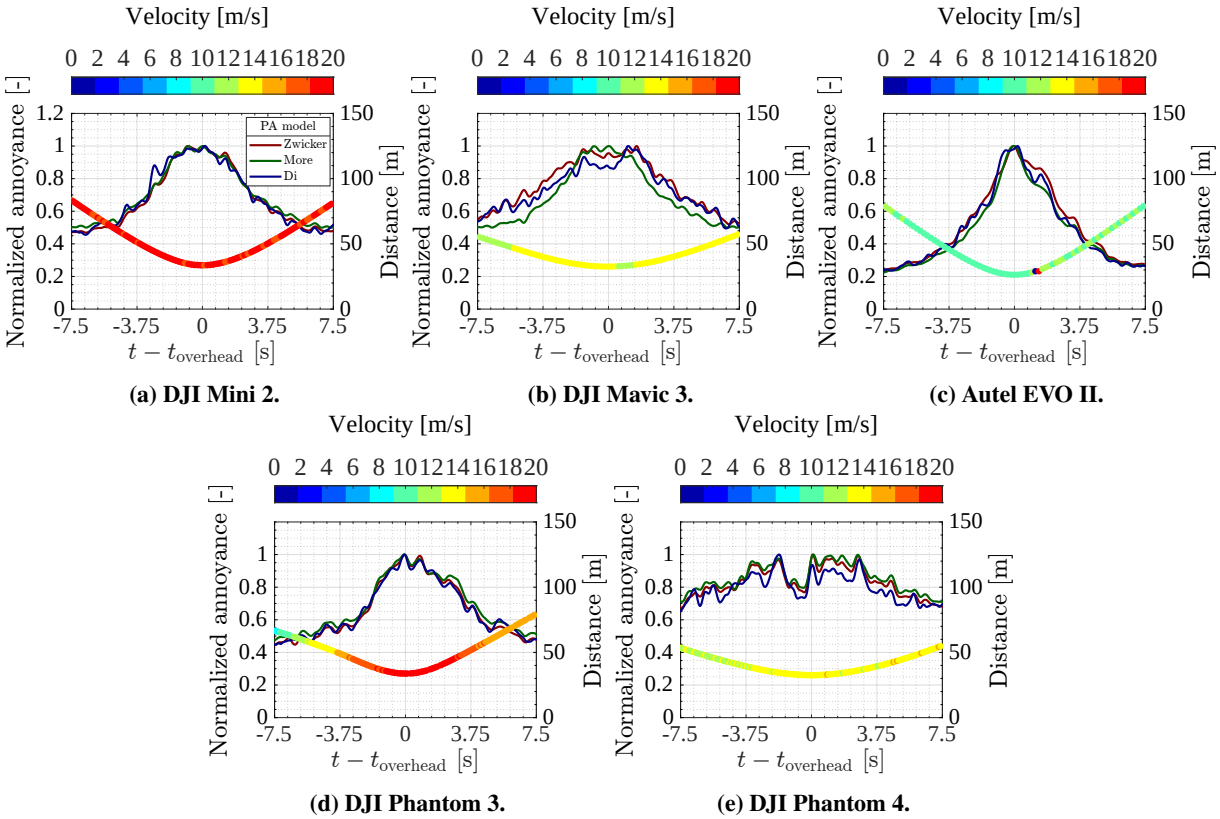

(a) DJI Mini 2. **(b) DJI Mavic 3.** **(c) Autel EVO II.**

(d) DJI Phantom 3. **(e) DJI Phantom 4.**

Fig. 11 Estimation of normalized annoyance during the flight missions.

Figure 12 shows a single normalized value of predicted annoyance with the maximum value in each annoyance model. In comparison with the previous analysis, the predicted annoyance from the Willemsen and Rao [36] model is also presented. For this analysis, the normalization involved dividing the 5th percentile values by the maximum value among the annoyances of each drone predicted by Zwicker and Fast [38], More [39], and Di et al. [40]. For the Willemsen and Rao [36] model, the same procedure is applied but using the cumulative impulsive content I_N. It can be seen that the drone 'Autel EVO II' (model 3) is perceived as the most annoying drone, while the 'DJI Phantom 4' (model 5) is assessed as the least annoying. Additionally, it is clearly noticeable that the Willemsen model predicts higher (normalized), and hence more similar to each other, values of annoyance in comparison to the other PA models. All the normalized annoyance values can be seen in Table 5.

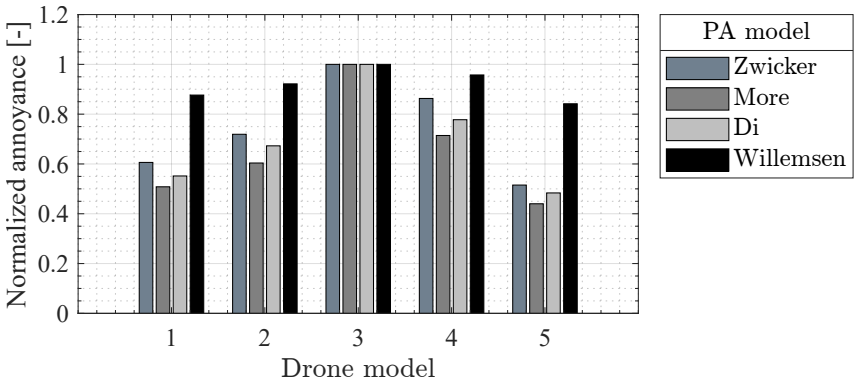

Fig. 12 Single values of normalized psychoacoustic annoyance.

Table 5 Summary of normalized psychoacoustic annoyance (PA) values predicted by the Zwicker, More, Di, and Willsemsen models.

Drone number	Drone model	Normalized annoyance [-]			
		Zwicker	More	Di	Willemsen
1	DJI Mini 2	0.60	0.50	0.55	0.87
2	DJI Mavic 3	0.72	0.60	0.67	0.92
3	Autel EVO II	1	1	1	1
4	DJI Phantom 3	0.86	0.71	0.78	0.96
5	DJI Phantom 4	0.51	0.44	0.48	0.84

3. Correlation between Annoyance and Drone Characteristics

Figure 13 depicts the linear regression analysis between the drone characteristics and the single normalized annoyance values according to each PA model. The drone characteristics are outlined in Table 6, while the single PA values are presented in Table 5. The analysis is conducted using the least squares method. It can be observed that the weight, volume, and propeller diameter do not exhibit a high degree of correlation with the single PA values, as the correlation coefficients obtained are low. For example, the highest correlation coefficients for the weight, propeller diameter, and volume are 0.298 (More PA model), 0.337 (Zwicker PA model), and 0.448 (More PA model), respectively. However, the parameters d (diagonal size) and d/D (installation ratio) demonstrate better correlations compared to the previous ones. The highest correlation corresponds to d/D with a value of 0.886 (More PA model), suggesting that this parameter not only affects the noise signature due to wake interaction [12] but also could influence psychoacoustic annoyance. The rest of the correlations presented very low correlation coefficients. Therefore, more measurements are required.

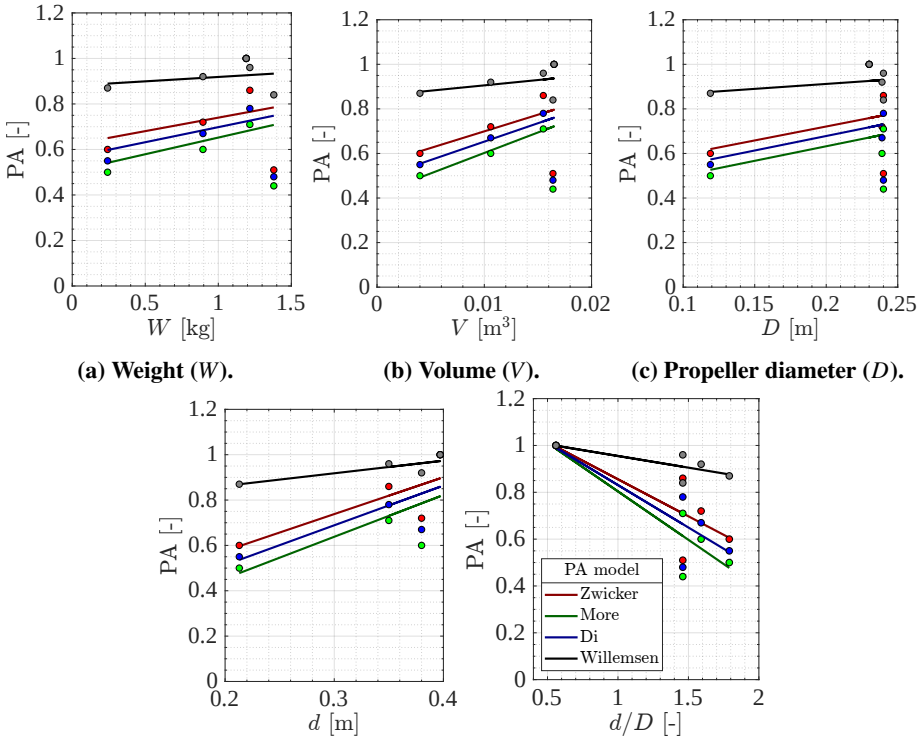

(a) Weight (W). **(b) Volume (V).** **(c) Propeller diameter (D).**

(d) Diagonal size (d). **(e) Installation ratio d/D.**

Fig. 13 Correlation between predicted annoyance with drone characteristics.

Table 6 Correlation coefficients (ρ) and p-value between the single annoyance values and the drone characteristics (on a linear scale). Statistically-significant (p-value < 0.05) correlation values are highlighted in bold.

Drone number	Drone characteristic	Zwicker PA model		More PA model		Di PA model		Willemsen PA model	
		ρ	p-value	ρ	p-value	ρ	p-value	ρ	p-value
1	Weight (W)	0.271	0.658	0.298	0.625	0.291	0.634	0.267	0.664
2	Volume (V)	0.409	0.495	0.448	0.449	0.434	0.465	0.396	0.509
3	Propeller diameter (D)	0.337	0.578	0.313	0.607	0.337	0.579	0.362	0.550
4	Diagonal size (d)	0.785	0.215	0.713	0.287	0.766	0.234	0.836	0.164
5	Installation ratio (d/D)	0.761	0.135	**0.886**	**0.04**	0.837	0.07	0.726	0.164

IV. Conclusions

This manuscript explored the acoustic and psychoacoustic characteristics of five different quadcopter drones under realistic flyover conditions. Outdoor acoustic recordings employed a 64-microphone array with a 4 m diameter. For the acoustic and psychoacoustic analyses, only a single single microphone was selected. The trajectories were adjusted to ensure a fairer comparison, with corrections made to account for sound spreading effects.

The acoustic analysis consisted in examine the signal-to-noise ratio (SNR), sound pressure levels in the time-frequency domain, and the noise spectra at the overhead position for each drone. Regarding the SNR, it was determined that the background noise does not mask the noise perception generated by the drones for frequencies higher than 100 Hz. Additionally, the maximum values of A-weighted SNR matched the instant at which the overhead position occurs, with the exception of the drone 'DJI Phantom 4'. Results of sound pressure levels in the time-frequency domain revealed significant noise levels up to 12 kHz, with the exception of the DJI Phantom 4 which presents higher noise levels up to 2.5 kHz. Moreover, multiple complex tones at the harmonics of the blade passage frequency (BPF) were observed as reported by the literature. Additionally, it was identified that the harmonics of the BPFs for each drone are predominantly noticeable up to 1 kHz. Unlike conventional fixed-wing aircraft, drones fly at much lower altitudes. As a result, atmospheric absorption, which typically reduces high-frequency noise, is less effective for drones because of their proximity to the ground.

The psychoacoustic analysis involved the assessment of sound quality metrics (SQMs), psychoacoustic annoyance (PA), and the correlation between annoyance and drone characteristics. Concerning the SQMs, density traces of the instantaneous values, as well as their 5th percentiles were analyzed. Sharpness, tonality, roughness, and impulsiveness exhibit similar transient density trace patterns, suggesting a consistent auditory signature across these attributes. However, the same coherence was not observed with loudness and fluctuation strength, as they fail to demonstrate comparable transient density trace patterns. In terms of perceived attributes, the heaviest drone was characterized as the 'harshest', 'least sharp', and 'quietest'. Conversely, the lightest drone is perceived as the 'sharpest', 'least harsh', and 'least impulsive'. The drone with the lowest installation ratio (d/D) was found to be the 'loudest', 'most tonal', 'most beating', and 'most impulsive'. Additionally, one of the drones with the largest propeller diameter is perceived as the 'least tonal'. Analyzing the transient psychoacoustic annoyance computed with the Zwicker, More, and Di models, it was observed that these values are strongly related to the distance between the drone's flight path and the microphone, as the annoyance reaches maximum levels around the overhead position. An analysis considering single values of psychoacoustic annoyance using the previous PA models and the Willemsem model indicated that the drone with the lowest d/D was perceived as the most annoying, while the heaviest model is assessed as the least annoying. Additionally, the Willemsen annoyance model predicted higher annoyance values in comparison to other PA models. Regarding the correlation between psychoacoustic annoyance and drone characteristics, it was shown that the installation ratio achieved a correlation coefficient of 0.836 (More PA model). This finding indicate that propeller positioning not only impacts noise signature due to wake interaction [12] but could also influence psychoacoustic annoyance.

V. Acknowledgments

This publication is part of the project *Listen to the future* (with project number 20247) of the research programme Veni 2022 (Domain Applied and Engineering Sciences) granted to Roberto Merino-Martinez which is (partly) financed by the Dutch Research Council (NWO).

References

[1] Floreano, D., and Wood, R. J., "Science, technology and the future of small autonomous drones," *nature*, Vol. 521, No. 7553, 2015, pp. 460–466. https://doi.org/10.1038/nature14542.

[2] Coleman, C., "UK expert report on drones," *Pwc report*, 2018.

[3] Hui, C. J., Kingan, M. J., Hioka, Y., Schmid, G., Dodd, G., Dirks, K. N., Edlin, S., Mascarenhas, S., and Shim, Y.-M., "Quantification of the psychoacoustic effect of noise from small unmanned aerial vehicles," *International Journal of Environmental Research and Public Health*, Vol. 18, No. 17, 2021, p. 8893. https://doi.org/10.3390/ijerph18178893.

[4] Gwak, D. Y., Han, D., and Lee, S., "Sound quality factors influencing annoyance from hovering UAV," *Journal of sound and vibration*, Vol. 489, 2020, p. 115651. https://doi.org/10.1016/j.jsv.2020.115651.

[5] Christian, A. W., and Cabell, R., "Initial investigation into the psychoacoustic properties of small unmanned aerial system noise," *23rd AIAA/CEAS aeroacoustics conference*, 2017, p. 4051. https://doi.org/10.2514/6.2017-4051.

[6] Zawodny, N. S., Boyd Jr, D. D., and Burley, C. L., "Acoustic characterization and prediction of representative, small-scale rotary-wing unmanned aircraft system components," Tech. rep., NASA, 2016.

[7] Thurman, C. S., "Computational study of boundary layer effects on stochastic rotor blade vortex shedding noise," *Aerospace Science and Technology*, Vol. 131, 2022, p. 107983. https://doi.org/10.1016/j.ast.2022.107983.

[8] Komasová, S., "Possible Inspiration: Drone-Related Literature and its Potential for Public Perception Research," *Journal of Intelligent and Robotic Systems*, 2021. https://doi.org/10.1007/s10846-021-01498-9.

[9] Wang, N., Mutzner, N., and Blanchet, K., "Societal acceptance of urban drones: A scoping literature review," *Technology in Society*, 2023, p. 102377. https://doi.org/10.1016/j.techsoc.2023.102377.

[10] Kephalopoulos, S., Paviotti, M., Anfosso-Lédée, F., Van Maercke, D., Shilton, S., and Jones, N., "Advances in the development of common noise assessment methods in Europe: The CNOSSOS-EU framework for strategic environmental noise mapping," *Science of the Total Environment*, Vol. 482, 2014, pp. 400–410. https://doi.org/10.1016/j.scitotenv.2014.02.031.

[11] White, K., Bronkhorst, A. W., and Meeter, M., "Annoyance by transportation noise: The effects of source identity and tonal components," *The Journal of the Acoustical Society of America*, Vol. 141, No. 5, 2017, pp. 3137–3144. https://doi.org/10.1121/1.4982921.

[12] Rizzi, S. A., Huff, D. L., Boyd, D. D., Bent, P., Henderson, B. S., Pascioni, K. A., Sargent, D. C., Josephson, D. L., Marsan, M., He, H. B., and Royce, S., "Urban air mobility noise: Current practice, gaps, and recommendations," Tech. rep., NASA, 2020.

[13] Breugelmans, O., Houthuijs, D., van Poll, R., Hajema, K., and Hogenhuis, R., "Predicting aircraft noise annoyance: Exploring noise metrics other than Lden," *12th ICBEN Congress on Noise as a Public Health Problem, June 12 – 18, Zurich, Switzerland*, 2017. URL http://www.icben.org/2017/ICBEN%202017%20Papers/SubjectArea08_Breugelmans_0802_3670.pdf.

[14] Merino-Martinez, R., Vieira, A., Snellen, M., and Simons, D. G., "Sound quality metrics applied to aircraft components under operational conditions using a microphone array," *25th AIAA/CEAS Aeroacoustics Conference, May 20 – 24 2019, Delft, The Netherlands*, 2019. https://doi.org/10.2514/6.2019-2513, URL http://arc.aiaa.org/doi/pdf/10.2514/6.2019-2513, AIAA paper 2019–2513.

[15] Torija, A. J., Roberts, S., Woodward, R., Flindell, I. H., McKenzie, A. R., and Self, R. H., "On the assessment of subjective response to tonal content of contemporary aircraft noise," *Applied Acoustics*, Vol. 146, 2019, pp. 190–203. https://doi.org/10.1016/j.apacoust.2018.11.015.

[16] Alkmim, M., Cardenuto, J., Tengan, E., Dietzen, T., Van Waterschoot, T., Cuenca, J., De Ryck, L., and Desmet, W., "Drone noise directivity and psychoacoustic evaluation using a hemispherical microphone array," *The Journal of the Acoustical Society of America*, Vol. 152, No. 5, 2022, pp. 2735–2745. https://doi.org/10.1121/10.0014957.

[17] Torija, A. J., Li, Z., and Self, R. H., "Effects of a hovering unmanned aerial vehicle on urban soundscapes perception," *Transportation Research Part D: Transport and Environment*, Vol. 78, 2020, p. 102195. https://doi.org/10.1016/j.trd.2019.11.024.

[18] Ramos-Romero, C., Green, N., Torija, A. J., and Asensio, C., "On-field noise measurements and acoustic characterisation of multi-rotor small unmanned aerial systems," *Aerospace Science and Technology*, Vol. 141, 2023, p. 108537. https://doi.org/10.1016/j.ast.2023.108537.

[19] Škultéty, F., Bujna, E., Janovec, M., and Kandera, B., "Noise Impact Assessment of UAS Operation in Urbanised Areas: Field Measurements and a Simulation," *Drones*, Vol. 7, No. 5, 2023, p. 314. https://doi.org/10.3390/drones7050314.

[20] Ko, J., German, B., and Rauleder, J., "Community Noise Impact of Multirotor Configurations During Landing Procedures," *AIAA AVIATION 2023 Forum*, 2023, p. 3362. https://doi.org/10.2514/6.2023-3362.

[21] Fastl, H., and Zwicker, E., *Psychoacoustics – Facts and models*, Third ed., Springer Series in Information Sciences, 2007. URL https://www.springer.com/gp/book/9783540231592, ISBN: 987–3–540–68888–4.

[22] Ko, J., Kim, Y., Jeong, J., and Lee, S., "Prediction-based psychoacoustic analysis of multirotor noise under gusty wind conditions," *The Journal of the Acoustical Society of America*, Vol. 154, No. 5, 2023, pp. 3004–3018. https://doi.org/10.1121/10.0022352.

[23] Torija, A. J., Chaitanya, P., and Li, Z., "Psychoacoustic analysis of contra-rotating propeller noise for unmanned aerial vehicles," *The Journal of the Acoustical Society of America*, Vol. 149, No. 2, 2021, pp. 835–846. https://doi.org/doi.org/10.1121/10.0003432.

[24] Torija, A. J., Li, Z., and Chaitanya, P., "Psychoacoustic modelling of rotor noise," *The Journal of the Acoustical Society of America*, Vol. 151, No. 3, 2022, pp. 1804–1815. https://doi.org/10.1121/10.0009801.

[25] Green, N., Torija, A. J., and Ramos-Romero, C., "Perception of noise from unmanned aircraft systems: Efficacy of metrics for indoor and outdoor listener positions," *The Journal of the Acoustical Society of America*, Vol. 155, No. 2, 2024, pp. 915–929.

[26] Altena, A., Luesutthiviboon, S., Croon, G. D., Snellen, M., and Voskuijl, M., "Comparison of Acoustic Localisation Techniques for Drone Position Estimation Using Real-World Experimental Data," IIAV CZECH s.r.o., 2023, pp. 1–8.

[27] Underbrink, J. R., "Circularly symmetric, zero redundancy, planar array having broad frequency range applications," , U.S. Patent number 6,205,224 B1. 2001. URL https://docs.google.com/viewer?url=patentimages.storage.googleapis.com/pdfs/US6205224.pdf.

[28] Merino-Martinez, R., Pieren, R., and Schäffer, B., "Holistic approach to wind turbine noise: From blade trailing–edge modifications to annoyance estimation," *Renewable and Sustainable Energy Reviews*, Vol. 148, No. 111285, 2021, pp. 1–14. https://doi.org/10.1016/j.rser.2021.111285, URL https://doi.org/10.1016/j.rser.2021.111285.

[29] Merino-Martinez, R., Pieren, R., Schäffer, B., and Simons, D. G., "Psychoacoustic model for predicting wind turbine noise annoyance," 24th *International Congress on Acoustics (ICA), October 24 – 28 2022, Gyeongju, South Korea*, 2022. URL https://www.researchgate.net/publication/364996997_Psychoacoustic_model_for_predicting_wind_turbine_noise_annoyance.

[30] Greco, G. F., Merino-Martinez, R., Osses, A., and Langer, S. C., "SQAT: a MATLAB-based toolbox for quantitative sound quality analysis," 52th *International Congress and Exposition on Noise Control Engineering, August 20 – 23 2023, Chiba, Greater Tokyo, Japan*, International Institute of Noise Control Engineering (I-INCE), ???? URL https://www.researchgate.net/publication/373334884_SQAT_a_MATLAB-based_toolbox_for_quantitative_sound_quality_analysis.

[31] "ISO norm 532–1 – Acoustics – Method for calculating loudness – Zwicker method," Tech. Rep. 1, International Organization for Standardization, 2017. URL https://www.iso.org/obp/ui/#iso:std:iso:532:-1:ed-1:v2:en.

[32] Aures, W., "Procedure for calculating the sensory euphony of arbitrary sound signal. In German: Berechnungsverfahren für den sensorischen Wohlklang beliebiger Schallsignale," *Acustica*, Vol. 59, No. 2, 1985, pp. 130–141. URL https://www.ingentaconnect.com/contentone/dav/aaua/1985/00000059/00000002/art00008.

[33] von Bismark, G., "Sharpness as an attribute of the timbre of steady sounds," *Acta Acustica united with Acustica*, Vol. 30, No. 3, 1974, pp. 159–172. URL https://www.semanticscholar.org/paper/Sharpness-as-an-attribute-of-the-timbre-of-steady-Bismarck/9576a2a74bff46ee0cded25bfd9e4302b4fb0470.

[34] Daniel, P., and Webber, R., "Psychoacoustical Roughness: Implementation of an Optimized Model," *Accustica – acta acustica*, Vol. 83, 1997, pp. 113–123. URL https://www.ingentaconnect.com/contentone/dav/aaua/1997/00000083/00000001/art00020.

[35] Osses, A., García León, R., and Kohlrausch, A., "Modelling the sensation of fluctuation strength," 22nd *International Congress on Acoustics (ICA), September 5 – 9 2016, Buenos Aires, Argentina*, 2016. URL https://pure.tue.nl/ws/portalfiles/portal/52366479/Osses_Garcia_Kohlrausch_ICA2016_ID113.pdf.

[36] Willemsen, A. M., and Rao, M. D., "Characterization of sound quality of impulsive sounds using loudness based metric," *20th International Congress on Acoustics*, 2010, pp. –.

[37] Boucher, M., Rafaelof, M., Begault, D., Christian, A., Krishnamurthy, S., and Rizzi, S., "A Psychoacoustic Test for Urban Air Mobility Vehicle Sound Quality," *INTER-NOISE and NOISE-CON Congress and Conference Proceedings*, Vol. 266, Institute of Noise Control Engineering, 2023, pp. 794–807.

[38] Zwicker, E., and Fastl, H., *Psychoacoustics: Facts and models*, Vol. 22, Springer Science & Business Media, 2013.

[39] More, S. R., "Aircraft noise characteristics and metrics," Ph.D. thesis, Purdue University, 2010.

[40] Di, G.-Q., Chen, X.-W., Song, K., Zhou, B., and Pei, C.-M., "Improvement of Zwicker's psychoacoustic annoyance model aiming at tonal noises," *Applied Acoustics*, Vol. 105, 2016, pp. 164–170. https://doi.org/10.1016/j.apacoust.2015.12.006, URL http://dx.doi.org/10.1016/j.apacoust.2015.12.006.

[41] Greco, G. F. and Merino-Martinez, R. and Osses, A., "SQAT: a sound quality analysis toolbox for MATLAB," , May 2023. URL https://github.com/ggrecow/sqat, accessed in May 2023.

[42] Alexander, W. N., and Whelchel, J., "Flyover noise of multi-rotor sUAS," *Inter-Noise and Noise-Con Congress and Conference Proceedings*, Vol. 259, Institute of Noise Control Engineering, 2019, pp. 2548–2558.

[43] Torija, A. J., Self, R. H., and Lawrence, J. L., "Psychoacoustic characterisation of a small fixed-pitch quadcopter," *Inter-Noise and Noise-Con Congress and Conference Proceedings*, Vol. 259, Institute of Noise Control Engineering, 2019, pp. 1884–1894.

[44] Cabell, R., Grosveld, F., and McSwain, R., "Measured noise from small unmanned aerial vehicles," *Inter-Noise and Noise-Con Congress and Conference Proceedings*, Vol. 252, Institute of Noise Control Engineering, 2016, pp. 345–354.

[45] Alexander, W. N., Whelchel, J., Intaratep, N., and Trani, A., "Predicting community noise of sUAS," *25th AIAA/CEAS Aeroacoustics Conference*, 2019, p. 2686.